Application of 3D-QSAR for Identification of Descriptors Defining Bioactivity of Antimicrobial Peptides

Jayendra B. Bhonsle,* Divakaramenon Venugopal, Donald P. Huddler, Alan J. Magill, and Rickey P. Hicks*

Division of Experimental Therapeutics, Walter Reed Army Institute of Research 503 Robert Grant Avenue, Silver Spring, Maryland 20910, USA

Received July 23, 2007

In our laboratory, a series of antimicrobial peptides have been developed, where the resulting 3D-physicochemical properties are controlled by the placement of amino acids with well-defined properties (hydrophobicity, charge density, electrostatic potential, and so on) at specific locations along the peptide backbone. These peptides exhibited different in vitro activity against *Staphylococcus aureus* (SA) and *Mycobacterium ranae* (MR) bacteria. We hypothesized that the differences in the biological activity is a direct manifestation of different physicochemical interactions that occur between the peptides and the cell membranes of the bacteria. 3D-QSAR analysis has shown that, within this series, specific physicochemical properties are responsible for antibacterial activity and selectivity. There are five physicochemical properties specific to the SA QSAR model, while five properties are specific to the MR QSAR model. These results support the hypothesis that, for any particular AMP, organism selectivity and potency are controlled by the chemical composition of the target cell membrane.

Introduction

Antimicrobial peptides (AMPs[a]) have evolved in almost every class of living organisms, functioning as a host defense mechanism against invading micro-organisms.[1,2] These peptides are generally small highly positively charged[3] molecules with well-defined hydrophobic and hydrophilic regions.[4,5] AMPs may be divided into two mechanistic super families as membrane-disruptors and nonmembrane-disruptors.[6,7] All membrane-disruptors are believed to follow specific steps in the process of interacting with and binding to the target cells or to model membranes.[8] The AMP is first attracted to the surface of the membrane[7] by the electrostatic interactions that occur between the positively charged amino acids of the AMP and the negatively charged phospholipids of the cell membrane.[1,9,10] The following step involves the binding of the AMP to the surface of the membrane.[7] It is becoming more accepted in the literature that it is the electrostatic interactions occurring between the target cell's membrane and the peptide that determines organism potency and selectivity.[1,2,4,6] It is well-known that bacterial cells contain a high percentage of negatively charged phospholipids, while mammalian cells contain a much higher concentration of zwitterionic phospholipids.[11] Therefore, the variation in the chemical composition of the respective membranes is a rational explanation for the observed selectivity of some AMPs for prokaryotic versus eukaryotic cells.[1,4]

We have extended this rationale to explain the observed differences in organism selectivity and potency for various bacterial strains as well. It is well-known that the chemical compositions of the membranes of different bacterial strains vary.[1,12,13] Because the chemical compositions of the membranes of different bacterial strains vary greatly, the resulting physicochemical surface properties presented by the membrane to the external environment will therefore be different as well as specific for each type of bacterial strain. Our guiding hypothesis evolved from the above assertion, which in its simplest form states the following: the 3D-physicochemical surface properties of target cell membrane (bacterial or mammalian) interact with the 3D-physicochemical surface properties of the approaching AMP in a very specific way (via bioactive conformation), thus defining the resulting organism selectivity and potency. If this hypothesis is correct, then the interactions of a closely related series of antimicrobial peptides against different bacterial strains should be described by different physicochemical descriptors.

Materials and Methods

Cerius2 (C2), version 4.9,[14] and InsightII, version 2000.1, running on a Silicon Graphics Octane workstation under IRIX 6.5 operating system, were used for all of the modeling calculations presented here. Gasteiger[15] charges ClassII force field[16] was used for all of the computations using C2, and consistent valence force field (CVFF) was used for all computations using InsightII. Unless otherwise noted, default C2 and InsightII parameters were used. For this investigation, 28 compounds (Table 1) previously synthesized and tested in our laboratory[17] were selected such that they ensured a diversity of activity against *Staphylococcus aureus* ME/GM/TC resistant (ATCC 33592) (SA) and *Mycobacterium ranae* (ATCC 110; MR) bacteria.

Molecular Structure Building, Conformational Search, Cluster Analysis and Descriptor Computation. Each peptide was constructed in the Biopolymer module of InsightII, energy minimized using steepest descent algorithm[18] and subjected to a brief (1000 cycles) MD simulation, followed by exhaustive minimization to give the local minimum conformation of the peptide. The

* To whom correspondence should be addressed. Ricky P. Hicks: Department of Chemistry, East Carolina University, Science and Technology Building, Suite 300, Greenville, NC 27858. Telephone: 252-328-9700. Fax: 252-328-6210. E-mail: hicksr@ecu.edu. For correspondence concerning molecular modeling protocols, etc., contact J. B. Bhonsle: Walter Reed Army Institute of Research. Telephone: 301-319-9060. Fax: 301-319-9449. E-mail: jayendra.bhonsle@na.amedd.army.mil.

[a]Abbreviations: Ahx, 6-aminohexanoic acid; AMP, antimicrobial peptide; βAla, β-alanine; CoMFA, comparative molecular field analysis; CtoBA, contribution to bioactivity; Dpr, diaminopropionic acid; DSP, descriptor significance percentage; ESP, electrostatic surface potential; Fpa, 4-fluorophenylalanine; Gaba, γ-aminobutyric acid; MD, molecular dynamics; MR, *Mycobacterium ranae*; Nph, 4-nitrophenylalanine; Oic, octahydroindolecarboxylic acid; PRES, prediction error sum; PRESS, prediction error sum squares; PLS, partial least-squares; QSAR, quantitative structure–activity relationship; Tic, tetrahydroisoquinolinecarboxylic acid; cmpd, compound; SA, *Staphylococcus aureus*; VDW, van der Waal radii.

10.1021/jm070884y CCC: $37.00
Published on Web 12/07/2007

Table 1. Peptide Amino Acid Sequence and Antibacterial Activity against *Staphylococcus aureus* (SA) and *Mycobacterium ranae* (MR)[a]

C#	amino acid sequence	SA μM[b]	MR μM[b]
1	NH_2-KL-Tic-Oic-K-Tic-Oic-F-Tic-Oic-K-Tic-Oic-F-Tic-Oic-K-Tic-Oic-KR-NH_2	10	30
2	Ac-GF-Tic-Oic-GK-Tic-Oic-GF-Tic-Oic-GK-Tic-KKKK-NH_2	3	10
3	NH_2-GF-Tic-Oic-GK-Tic-Oic-GF-Tic-Oic-GK-Tic-KKKK-NH_2	10	10
4	NH_2-KL-Tic-Oic-GK-Tic-Oic-GF-Tic-Oic-GK-Tic-KKKK-NH_2	30	3
5	Ac-F-Tic-Oic-K-Tic-Oic-F-Tic-Oic-K-Tic-KKKK-NH_2	3	30
6	Ac-F-Tic-Oic-K-Tic-Oic-F-Tic-Oic-K-Tic-KKKKKK-NH_2	3	3
7	Ac-Gaba-F-Tic-Oic-Gaba-K-Tic-Oic-Gaba-F-Tic-Oic-Gaba-K-Tic-KKKK-NH_2	100	10
8	Ac-βAla-F-Tic-Oic-βAla-K-Tic-Oic-βAla-F-Tic-Oic-βAla-K-Tic-KKKK-NH_2	10	1
9	Ac-Ahx-F-Tic-Oic-Ahx-K-Tic-Oic-Ahx-F-Tic-Oic-Ahx-K-Tic-KKKK-NH_2	10	3
10	Ac-Gaba-F-Tic-Oic-Gaba-K-Tic-Oic-Gaba-F-Tic-Oic-Gaba-K-Tic-KKKKK-NH_2	30	3
11	Ac-G-Tic-Oic-K-Tic-Oic-G-Tic-Oic-K-Tic-KKKK-NH_2	10	3
12	Ac-GF-Oic-GK-Oic-GF-Oic-GKKKKK-NH_2	10^6	100
13	Ac-GF-G-Oic-GK-G-Oic-GF-G-Oic-GK-G-KKKK-NH_2	10^6	100
14	Ac-GF-Tic-GK-Tic-GF-Tic-GK-Tic-KKKK-NH_2	10^6	30
15	*Ac*-GF-Tic-G-GK-Tic-G-GF-Tic-G-GK-Tic-KKKK-NH_2	10^6	30
16	Ac-GF-F-Oic-GK-F-Oic-GF-F-Oic-GK-F-KKKK-NH_2	10	10
17	Ac-GF-Tic-Oic-GK-Tic-Oic-GF-Tic-Oic-GK-Tic-KKKKK-NH_2	3	3
18	Ac-GF-Tic-Oic-GK-Tic-Oic-GF-Tic-Oic-GK-Tic-OOOO-NH_2	10	10
19	Ac-G-Fpa-Tic-Oic-GK-Tic-Oic-G-Fpa-Tic-Oic-GK-Tic-KKKK-NH_2	10	3
20	Ac-GF-Tic-Oic-GO-Tic-Oic-GF-Tic-Oic-GO-Tic-OOOO-NH_2	3	10
21	Ac-GF-Tic-Oic-GK-Tic-Oic-GF-Tic-Oic-GK-Tic-KKKK-CONH-CH_2-CH_2-NH_2	3	10
22	Ac-GF-Tic-Oic-GK-Tic-Oic-GF-Tic-Oic-GK-Tic-KKKK-CONH-CH_2-CH_2-CH_2-NH_2	10	10
23	NH_2-ELMNS-Tic-Oic-GL-Tic-Oic-GK-Tic-Oic-GL-Tic-Oic-GK-Tic-Oic-ELMNS-NH_2	10^6	10^6
24	NH_2-GKGL-Tic-Oic-GK-Tic-Oic-GF-Tic-Oic-GK-Tic-Oic-GF-Tic-Oic-GK-Tic-Oic-GKR-NH_2	10	NT
25	NH_2-GKGL-Tic-Oic-GR-Tic-Oic-GF-Tic-Oic-GR-Tic-Oic-GF-Tic-Oic-GR-Tic-Oic-GKR-NH_2	10	10^6
26	NH_2-GKGL-Tic-Oic-GL-Tic-Oic-GK-Tic-Oic-GL-Tic-Oic-GK-Tic-Oic-GL-Tic-Oic-GLR-NH_2	100	NT
27	NH_2-GKGL-Tic-Oic-GK-Tic-Oic-GL-Tic-Oic-GK-Tic-Oic-GL-Tic-Oic-GK-Tic-Oic-GKR-NH_2	10	NT
28	NH_2-GKGL-Tic-Oic-FK-Tic-Oic-KF-Tic-Oic-FK-Tic-Oic-KF-Tic-Oic-FK-Tic-Oic-FKR-NH_2	30	10^6

[a] C# = cmpd #; Fpa = 4-fluoro phenylalanine; Gaba = γ-aminobutyric acid; Ahx = ϵ-aminohexanoic acid; Ac = acetyl; NT = not tested. [b] All analogs were screened in the concentration range of 0.1 μM to 100 μM; therefore, active compounds exhibited MIC of <100 μM. For computational purposes, all inactive compounds were deemed to have an MIC of 1.0 M.

conformational search was carried out using Boltzmann jump or Monte Carlo algorithm.[19] The parameters for Boltzmann jump used were as follows: number of conformations = 2000; torsion window = 120; number of perturbations = 50; and temp = 5000 K. Conformations differing less than 1.0 Å (rmsd) and energy values larger than 1000 kcal/mol were discarded. The conformations were clustered using the root mean squares (rms) difference of the torsion angles of the peptides[20] to yield preliminary clusters of 10–20, 20–30, 30–40, and 40–50 conformers per cluster. The steps in the conformer clustering algorithm[20] are as follows: all of the conformers are sorted by energy. The lowest-energy conformer is assigned to the first cluster and it becomes the cluster nuclei. Next, all the conformers that have a rms difference below the specified threshold value are placed in the first cluster. The lowest-energy conformer of the remaining unclustered conformers is placed in the second cluster as its cluster nuclei. Again, all the conformers that have a rms difference below the specified threshold value are placed in the second cluster. The above two steps are repeated until all the conformers are placed into clusters. The clusters with the best three-dimensional spatial representations, as determined by visual inspection to be with 20–30 conformers for some and 30–40 conformers for the rest, were selected. We used Tcl-based Cerius2 scripts[21,22] to automate the repetitive task of conformational searches and cluster analyses. All the conformers of all the peptides were aligned and added to a study table for descriptor computation with default settings. The correlation matrix was computed for all the descriptor values of all the conformers of all peptides to obtain the cross correlation and correlation with bioactivity coefficients.

Quasi-Multiway PLS Analyses. The partial least-squares (PLS) method[23] is used when the number of independent variables (descriptors) greatly exceeds the number of experimental observations and there is colinearity among independent variables. The following PLS parameters were used unless specified otherwise: The complexity of the model was limited to a six-component system, and the resulting descriptors were normalized to their mean value. The definitions of the statistical terms used are as follows:

Equation 1 gives the conventional correlation coefficient or the nonvalidated correlation coefficient r^2

$$r^2 = 1 - \left[\left(\sum (Y - Y_{\text{pred}})^2\right)/\left(\sum (Y - Y_{\text{mean}})^2\right)\right] \quad (1)$$

where Y is the observed bioactivity, Y_{pred} is the predicted bioactivity, and Y_{mean} is the mean bioactivity of all the training set compounds.

Equation 2 gives the cross-validation correlation coefficient q^2.

$$q^2 = 1 - \left[\left(\sum (Y - Y_{\text{CVpred}})^2\right)/\left(\sum (Y - Y_{\text{mean}})^2\right)\right] \quad (2)$$

where Y_{CVpred} is the cross-validated predicted bioactivity.

Equation 3 gives the predictive correlation coefficient r^2_{pred}.

$$r^2_{\text{pred}} = (\text{SD} - \text{PRES})/\text{SD} \quad (3)$$

where SD is the sum of squared deviations between the bioactivity of compounds in the test set and the mean bioactivity of the training set compounds and PRES is the sum of the squared deviation between the predicted and observed bioactivity for every test set compound.

Prediction error sum of squares (PRESS) for the training set compounds is given by equation 4.

$$\text{PRESS} = \sum (Y - Y_{\text{pred}})^2 \quad (4)$$

The multiway-PLS method was first reported by Bro et al.[24] Hasegawa et al.[25] have reported the application of the multiway-PLS method for 3D-QSAR model development of neonictinoid insecticidal compounds. Each dimension of the multiway data corresponded to the compounds in the training set, CoMFA field variables, conformations, and alignments, respectively. The conformers and alignments that gave the best correlation to the observed bioactivities were determined from the multiway-PLS solution. We have mimicked the multiway-PLS analyses by performing several sequential two-way PLS analyses on our data. We used a Tcl-based Cerius2 script[26] to automate the repetitive task of several PLS analyses.

Computation of Electrostatic Surface Potential Maps. Electrostatic surface potential maps for salient AMP conformers were

computed as follows. The electrostatic potential for each conformer was computed employing a grid with origin at its grid points, resolution of 65 points per axis and solute extending to 80 Å. The solute was defined with Gasteiger charges, VDW radii (van der Waal radii), dielectric constant of 2.0, and point charge distribution. The solvent dielectric constant was set to 80, the solvent radii was set to 1.4 Å, the ionic strength was set to 0.145, and the ionic radii was set to 2.0 Å. The molecular surfaces computed were Connolly surfaces with solid display style, using the default atom radii scale of 1.0 and probe radius of 1.4 Å. The surfaces were colored with Delphi spectrum using the electrostatic potential grid as the coloring method.

Results

The conformational search and cluster analysis data is summarized in Supplementary Table 1. A total of 50 different 2D and 3D descriptors were calculated for all the conformers. The list of descriptors is shown in Supporting Information, Table 2. The final selection of the significant descriptors is an important first step in QSAR analysis. Several techniques for descriptor selection to reduce dimensionality have been reported,[27,28] however, we employed the strategy reported by Yao et al.[29] The cross correlation matrix for the two models, namely, *Staphylococcus aureus* (SA), and *Mycobacterium ranae* (MR) was used for descriptor selection. The descriptors that showed very poor correlation with bioactivity ($r < 0.01$) were removed. Supporting Information, Table 3, shows the discarded descriptors and their correlation coefficients with bioactivity for the two models. The cross-correlation matrix showed that 33 descriptors exhibited very high cross-correlation coefficient values ($r > \sim 0.9$). Supporting Information, Table 4, summarizes the highly collinear descriptor types, names, and their cross-correlation coefficient values.

The final 22 and 21 descriptors for SA and MR QSAR models were selected, employing the following method and rationale. First, the descriptors were sorted based on their correlation coefficient with bioactivity. Next, those descriptors with more physical significance to offer mechanistic insight in the QSAR information were retained and selections were made from the highly collinear descriptors. For example for the SA model, given a choice between Jurs-SASA, PMI-Mag, RadOfGyration, Jurs-WNSA-1, and Jurs-WPSA-1, the Jurs-SASA was retained because it provides information about the effect of the total solvent accessible surface area on overall bioactivity. Table 2 shows the list of final descriptors used for the two QSAR models.

Our novel bioactive conformer mining methodology mines the clustered conformations to identify the conformer that most closely correlates with bioactivity. Further, the use of the gradual and stepwise refinement gives a steady enrichment of bioactive conformers in each successive model generation. This methodology has been demonstrated to deliver highly predictive QSAR models for cyclic pentapeptide CXCR4 inhibitors[21] and insect repellents.[30] The flowchart of the bioactive conformation mining algorithm is depicted in Supporting Information, Figure 1.

The bioactive conformer mining method, over seven iterative generations[21,27] resulted in two conformers each for the 12 peptides (cmpd no. **1**, **2**, **5**, **6**, **17**, **19**, **20**−**22**, **24**, **25**, and **27** for SA and cmpd. no. **4**, **6**, **8**−**11**, and **17**−**22** for MR) and one conformer for each the remaining 16 peptides. The details of these seven generations of QSAR models are shown in Supporting Information, Table 5. The best set of 12 conformers, from the 24 conformers, could be selected in 4096 (2^{12}) ways. A Tcl-based Cerius2 script[26] was used to compute these 4096 eighth-generation models. The final SA and MR QSAR model showed nonvalidated r^2 of 0.988 and 0.997, leave-one-out cross-validated r^2 of 0.839 and 0.997, with PRESS values of 22.92 and 29.19, respectively. The QSAR equations defining the activity against SA is given in eq 1 and against MR is given in eq 2. The correlation plots of the predicted versus the observed antibacterial activities of these two QSARs are given in Figure 1). The details of the QSAR models, such as the selected conformers, predicted bioactivities, and residual prediction errors are shown in Supporting Information, Tables 6 and 7 for SA and MR QSAR models, respectively.

Table 2. Rank Ordering of the Physicochemical Properties Defining Antibacterial Activity

physico-chemical property	*Staphylococcus aureus* QSAR_DSP	physico-chemical property	*Mycobacterium ranae* QSAR_DSP
Jurs-FPSA-1	29.347	density	−30.784
density	−16.01	Jurs-RASA	16.827
Jurs-TASA	−14.762	Jurs-PPSA-1	−15.494
Jurs-PNSA-1	10.54	Jurs-TPSA	10.218
Jurs-RASA	7.886	Jurs-RPSA	−5.444
Jurs-SASA	4.12	Hbond donor	−3.905
Jurs-DPSA-2	3.093	Hbond acceptor	3.729
Jurs-PNSA-2	−2.911	Jurs-FPSA-1	−3.409
Jurs-RPSA	−2.492	Fcharge	2.892
Rotlbonds	−2.164	Jurs-PNSA-1	−1.244
Hbond acceptor	1.91	RadOfGyration	1.164
Jurs-FPSA-3	1.709	Rotlbonds	−1.156
Fcharge	−0.742	Apol	1.148
Jurs-RPCG	−0.726	Jurs-PPSA-2	1.016
Jurs-PPSA-1	0.555	Jurs-PNSA-2	−0.632
Jurs-FNSA-3	−0.426	Jurs-RNCG	0.4
dipole-mag	0.162	dipole-mag	0.298
RadOfGyration	−0.127	Jurs-FNSA-3	−0.127
Jurs-RPCS	−0.126	AlogP	0.051
Hbond donor	0.113	conformer energy	0.037
Jurs-DPSA-3	0.053	Jurs-RPCG	−0.024
AlogP	−0.026	Jurs-DPSA-2	0

Internal validation (cross-validation) tests of the selected QSAR models were performed at two levels. Both of the models showed $q^2_{LOO} > 0.83$ for the leave-one-out (LOO) cross-validation tests. For the leave-10%-out or leave-three-out (L10O) cross-validation tests, the SA model showed q^2_{L10O} of 0.875, whereas the MR model showed q^2_{L10O} values of 0.537. It is known that even with large number of observations and fewer terms, the QSAR models can be poorly predictive.[31] The propensity for this chance correlation is assessed by the randomization test, where the dependent variables (bioactivity) are randomly reassigned to different compounds and a new regression model is recomputed, with the process being repeated several times. If the statistical data of these randomized models are comparable to the computed QSAR model, then the QSAR model is not predictive and the number of observations is insufficient. We performed randomization tests of 99 trials, each at 99% confidence level for SA and MR QSAR models. None of the random r values were found to be larger than the nonrandom r values for either the SA or the MR models. The mean random r value for the SA model was 0.572 ($r^2 = 0.327$), and for the MR model, the mean random r value was 0.617 ($r^2 = 0.380$). This indicates that the SA and MR QSAR models are not obtained by chance.

Discussion

The 17 physiochemical properties common to the SA and MR QSAR models are shown in Table 2. The five physicochemical properties specific to the SA QSAR model are Jurs-fractional-positive-surface-area-3 (Jurs-FPSA-3), Jurs-relative-

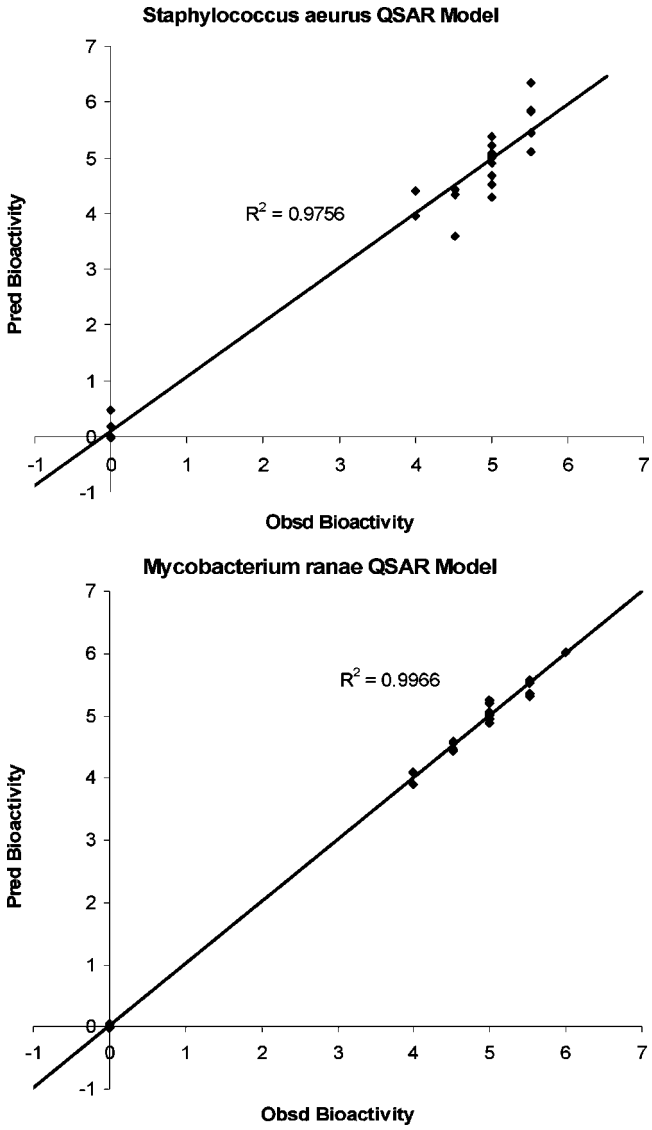

Figure 1. The correlation plot of predicted vs observed antibacterial activities of the two QSAR models.

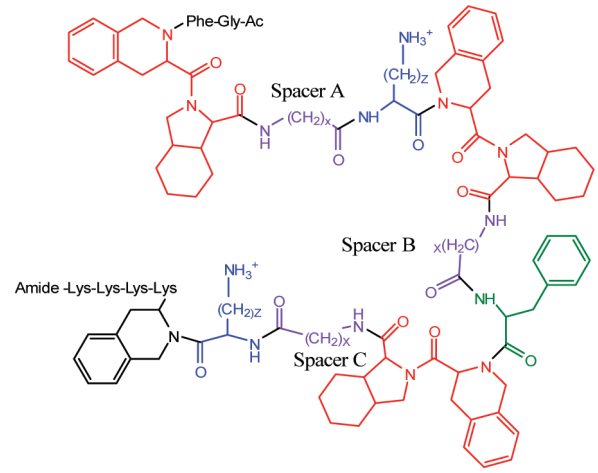

Figure 2. Tic-Oic dipeptide turn inducing unit is shown in red. The hydrophobic amino acid residues should exhibit hydrophobicity between −1.0 and −3.0 on the octanol scale.[34] Spacers A, B, and C are given in purple. Amino acid residues used as spacers A, B, and C should exhibit hydrophobicity between 1.2 and −0.75 on the octanol scale. The cationic residues are shown in blue. The cationic amino acid residues should exhibit hydrophobicity between 1.5 and 3.0 on the octanol scale. The hydrophobic amino acid residues are shown in green and should exhibit hydrophobicity between −1.0 and −3.0 on the octanol scale.

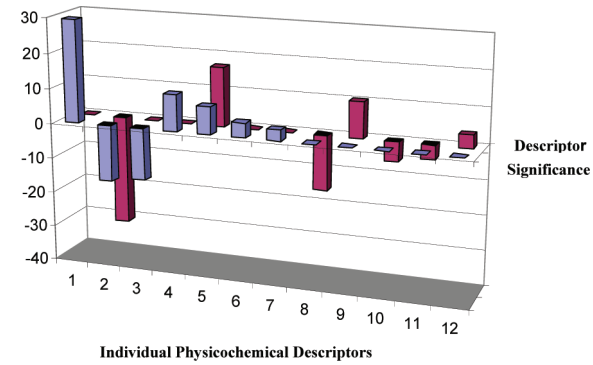

Figure 3. 3D graph of the seven most important 3D-physicochemical descriptor properties for each QSAR model. Descriptors for the SA model are shown in light blue and the descriptors for MR model are shown in purple. The *x*-axis indicates the individual descriptor physicochemical properties: (1) Jurs-FPSA-1, (2) density, (3) Jurs-TASA, (4) Jurs-PNSA-1, (5) Jurs-RASA, (6) Jurs-SASA, (7) Jurs-DPSA-2, (8) Jurs-PPSA-1, (9) Jurs-TPSA, (10) Jurs-RPSA, (11) H-bond donor, and (12) H-bonds acceptor. Only density and Jurs-RASA descriptors are common to both of the QSAR models. Each QSAR has five unique descriptors. The *y*-axis represents the descriptor significance percentage (DSP), which represents the quantitative contribution of any physicochemical property to the bioactivity of the respective descriptor.

positive-charge-surface-area (Jurs-RPCS), Jurs-differential-positively-charged-surface-area-3 (Jurs-DPSA-3), Jurs-total-solvent-accessible-surface-area (Jurs-SASA), and Jurs-total-hydrophobic-surface-area (Jurs-TASA). While the five physicochemical properties specific to the MR QSAR model are sum-of-all-atomic-polarizabilities (Apol), conformer energy, Jurs-partial-positively-charged-surface-area-2 (Jurs-PPSA-2), Jurs-relative-negative-charge (Jurs-RNCG), and Jurs-total-polar-surface-area (Jurs-TPSA). The commonality of physicochemical properties shows the minimal requirement for activity against SA and MR. A comparison of relative importance of these 10 descriptors is shown in Figure 3, which clearly indicates that different physicochemical properties define the activity of these AMPs for the two bacterial strains.

The physicochemical properties such as dipole-magnitude (dipole-mag), formal charge (Fcharge), Jurs-fractional-negatively-charged-surface-area (Jurs-FNSA-3), Jurs-relative-polar-surface-area (Jurs-RPSA), Jurs-fractional-positive-surface-area-1 (Jurs-FPSA-1), Jurs-fractional-negative-surface-area-1 (Jurs-PNSA-1), Jurs-fractional-negative-surface-area-2 (Jurs-PNSA-2), Jurs-partially-positive-surface-area-1 (Jurs-PPSA-1), and Jurs-relative-positive-charge (Jurs-RPCG) indicate the importance of electrostatic potential for the AMP bioactivity. While the physicochemical properties, such as molecular density (density), number-of-H-bond acceptors (H-bond acceptor), Jurs-relative-hydrophobic-surface-area (Jurs-RASA), number-of-H-bond donors (H-bond donor), molecular-radius-of-gyration (RadOfGyration), and number-of-rotatable-bonds (Rotlbonds), indicate the significance of the AMP molecular shape for bioactivity, the importance of amphipathicity is alluded to by the physicochemical properties, such as Jurs-RASA, Jurs-RPSA, and AlogP.

The QSAR equation shows the positive or negative contribution of various descriptors via the coefficients. However, the contributions of various descriptors in relation to each other can only be ascertained by taking into account the magnitude

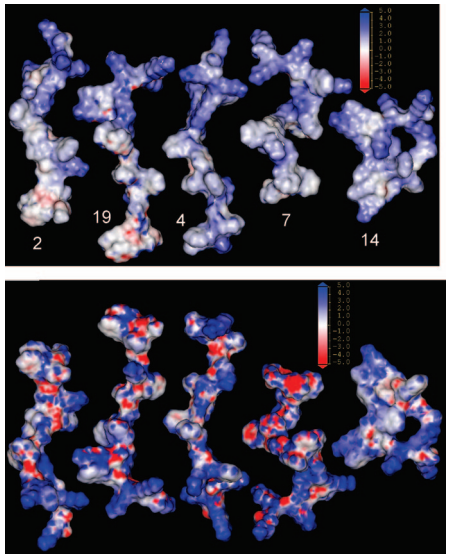

Figure 4. The ESP maps of five representative bioactive conformers used to generate 3D-QSAR for *Staphylococcus aureus*. For clarity, the MIC against *Staphylococcus aureus* (ME/GM/TC resistant) bacteria is given in parenthesis for each compound. Going from left to right, compound **2** (3 μM), compound **19** (10 μM), compound **4** (30 μM), compound **7** (100 μM), and compound **14** (in active). The top figure shows the nonpolar faces of these conformers, while the bottom figure shows the diametrically opposite polar faces of these conformers. Color coding: blue indicates positive potential, red indicates negative potential, and white indicates neutral potential.

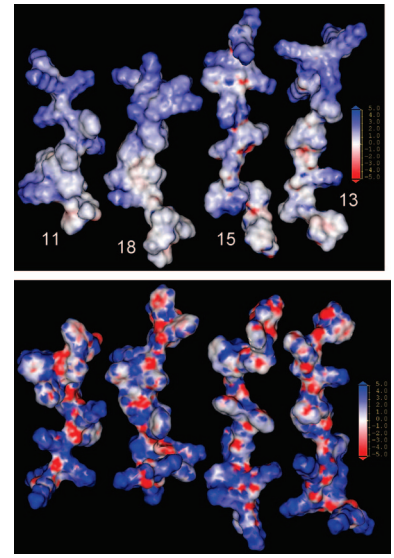

Figure 5. The ESP maps of four representative bioactive conformers used to generate 3D-QSAR for *Mycobacterium ranae*. For clarity, the MIC against *Mycobacterium ranae* bacteria is given in parenthesis for each compound. Going from left to right, compound **11** (3 μM), compound **18** (10 μM), compound **15** (30 μM), and compound **13** (100 μM). The top figure shows the nonpolar faces of these conformers, while the bottom figure shows the diametrically opposite polar faces of these conformers. Color coding: blue indicates positive potential, red indicates negative potential, and white indicates neutral potential.

of the descriptor values. We have coined the term descriptor significance percentage (DSP) to compute the contribution of each descriptor toward the overall bioactivity. The definition of DSP is as follows: the descriptor mean value is calculated as descriptor mean = descriptor values of all training set compounds/total number of compounds in the training set. The product of the QSAR coefficients and the respective descriptor mean value provides the contribution value of that descriptor to the overall bioactivity (contribution to bioactivity or CtoBA). Thus, CtoBA = QSAR_coefficient × descriptor_mean_value. The significance of CtoBA of any descriptor in relation to the CtoBA of all the other descriptors is computed by dividing the individual CtoBA by the sum total of all the CtoBA of all descriptors. The percentage value of this quotient is termed as "descriptor significance percentage or DSP". Thus, DSP = [(CtoBA × 100)/Σ abs(CtoBA)]. A positive DSP indicates that the descriptor increases antibacterial activity. A negative DSP indicates that the descriptor decreases antibacterial activity.

The DSP computation details for SA and MR QSAR models are presented in Supporting Information, Tables 8 and 9, respectively. The top six descriptors (DSP; Figure 3), namely, Jurs-FPSA-1 (29.35%), density (−16.01%), Jurs-TASA (−14.76%), Jurs-PNSA-1 (10.54%), Jurs-RASA (7.89%), and Jurs-SASA (4.12%), account for 82% of the SA predicted activity. To pictorially demonstrate the significance of electrostatics and sterics in the SA activity, we selected five representative AMPs: **2** (3μM), **19** (10μM), **4** (30μM), **7** (100μM), and **14** (inactive) from the various activity classes. The electrostatic surface potential (ESP) map of these AMPs, colored using the Delphi spectrum, shown in Figure 4, indicates that all AMPs have a distinct polar and nonpolar face. The correlation of nonpolar surface area to bioactivity is evident from the descriptors, such as Jurs-TASA with −14.76% DSP contribution and Jurs-RASA with 7.89% DSP contribution. The active AMPs (MIC < 100 μM) show more polar surface area than the inactive analog **14**. The high polar surface area correlation with bioactivity is evident by the Jurs-FPSA-1, with 29.4% DSP contribution and Jurs-PNSA-1 with 10.5% DSP contribution. The shape of the AMPs is critical for bioactivity, as seen in Figure 4. A loose helical shape is required for activity. A globular shape, as that of **14**, relates to loss of SA bioactivity. The shape correlation to bioactivity is illustrated by the descriptor density, with −16.01% DSP contribution and Jurs-SASA with 4.12% DSP contribution.

The significant descriptors accounting for 82% of MR predicted activity are density (−30.78%), Jurs-RASA (16.83%), Jurs-PPSA-1 (−15.49%), Jurs-TPSA (10.22%), Jurs-RPSA (−5.44%), and H-bond donor (−3.91%). A demonstration of the implication of electrostatics, sterics, hydrophobicity, and hydrophilicity is shown in Figure 5 for four representative AMPs, namely, **11** (3 μM), **18** (10 μM), **15** (30 μM), and **13** (100 μM). The correlation of the polar surface area to the MR bioactivity is evident from the descriptors Jurs-PPSA-1 with −15.5% DSP, Jurs-TPSA with 10.5% DSP contribution, and Jurs-RPSA with −5.44% DSP contribution. The hydrophobicity and hydrophilicity correlation with the MR bioactivity is shown by the descriptors Jurs-RASA with 16.8% DSP contribution and H-bond donor with −3.9% DSP. The contribution of shape to MR predicted bioactivity comes from the descriptor density with −30.78% DSP contribution. The two major structural variables in this study are (1) the Tic-Oic dipeptide and (2) the spacers A and B (refer Figure 2. The Tic-Oic dipeptide unit, which is critical for antibacterial activity, exhibits the greatest effect on the physicochemical properties via the following descriptors: (A) electrostatic potential: dipole-mag, Jurs-FNSA-3, Jurs-PNSA-1, Jurs-PNSA-2; (B) molecular shape: H-bond donor, RadOfGyration, Rotlbonds; and (C) amphipathicity: Jurs-RPSA, AlogP. As previously stated, the physicochemical properties, such as dipole-mag, Fcharge, Jurs-FNSA-3, Jurs-RPSA, Jurs-FPSA-1, Jurs-PNSA-1, Jurs-PNSA-2, Jurs-PPSA-1, and Jurs-RPCG, indicate the importance of electrostatics for the AMP bioactivity, while the physicochemical properties, such as density, H-bond acceptor, Jurs-RASA, H-bond donor, RadOf-

Table 3. Descriptors most Affected by the Tic-Oic Dipeptide Unit

	cmpd **2**		cmpd **12**		cmpd **13**		cmpd **14**		cmpd **15**		
cmpd	value	Δ%	value	Δ%	value	Δ%	value	Δ%	value	Δ%	Δ%
					Electrostatic Potential						
dipole-magnitude	269.60	0	251.73	−6.6	273.75	+1.5	81.00	−69.95	297.77	+10.45	80.4
F-charge	6.00	0	6.00	0	6.00	0	6.00	0	6.00	0	0
Jurs-FNSA-3	−0.05	0	−0.06	−20	−0.04	+20	−0.03	+40	−0.04	+20	60
Jurs-RPSA	0.27	0	0.33	+22.2	0.30	+11.1	0.26	−3.7	0.27	0	25.90
Jurs-FPSA-1	0.82	0	0.83	+1.2	0.82	0	0.81	−1.2	0.78	−4.87	6.07
Jurs-PNSA-1	576.30	0	446.76	−22.47	565.76	−1.8	503.61	−12.6	713.07	+23.7	46.17
Jurs-PNSA-2	−15950.51	0	−9781.01	+38.67	−8051.80	+49.52	−6499.05	+59.2	−10525.42	+34.0	59.20
Jurs-PPSA-1	2672.17	0	2225.44	−16.7	2513.86	−5.95	2136.09	−20.06	2459.00	−7.97	20.06
Jurs-RPCG	0.01	0	0.02	100	0.01	0	0.01	0	0.01	0	100
					Molecular Shape						
density	1.05	0	1.03	−1.9	1.05	0	1.06	+0.95	1.07	+1.9	3.80
H-bond acceptor	20.00	0	16.00	−20	20.00	0	17.00	−15	20.00	0	40
Jurs-RASA	0.73	0	0.67	−8.2	0.70	−4.1	0.74	+1.4	0.73	0	9.60
H-bond donor	32.00	0	32.00	0	36.00	+12.5	32.00	0	35.00	+9.4	12.50
Rad-of-gyration	14.55	0	13.47	−7.4	15.88	+9.1	10.18	−30.0	16.79	+15.39	45.39
Rotl-bonds	78.00	0	70.00	−10.25	82.00	+5.1	72.00	−7.69	81.00	+3.85	15.35
					Amphipathicity						
Jurs-RASA	0.73	0	0.67	−8.2	0.70	−4.1	0.74	+1.4	0.73	0	9.60
Jurs-RPSA	0.27	0	0.33	+22.2	0.30	+11.1	0.26	−3.7	0.27	0	+25.90
AlogP	−3.25	0	−7.75	−138	−12.05	−270.7	−5.85	−80	−9.08	−179.3	270

Gyration, and Rotlbonds, indicate the significance of the AMP molecular shape for bioactivity. The importance of amphipathicity is alluded to by the physicochemical properties, such as Jurs-RASA, Jurs-RPSA, and AlogP. The calculated values for these descriptors for each of the salient compounds are given in Table 3. Compound **2** was selected based on its broad spectrum activity (activity against *Staphylococcus aureus* ME/GM/TC resistant at 3 μM and *Mycobacterium ranae* at 10 μM concentration coupled with relatively low hemolytic activity at 14%) as the reference compound for this investigation. In addition, the % deviation (Δ%) from the value for compound **2** and a % range (Δ% range) deviation for the series of compounds is also given. The effect of deleting either the Tic or Oic residue on the conformational flexibility of the resulting peptide is shown in Figure 6. The calculated "bioactive" conformers of these analogs are extended and do not include a helical or β-turn structure. Preliminary CD studies (data not shown) indicate that in aqueous buffer these analogs exhibit characteristics of a random coil conformer.

The effect of spacers A and B on the physicochemical properties via various descriptors may be summarized as follows: (A) electrostatic potential: dipole-mag, Jurs-FNSA-3, Jurs-RPSA, Jurs-PNSA-1, Jurs-PNSA-2, Jurs-PPSA-1; (B) molecular shape: Rotlbonds; (C) amphipathicity: Jurs-RPSA, AlogP. The calculated values for these descriptors for each of the salient compounds are given in Table 4. The statistically significant differences are highlighted in bold face. The physicochemical properties and the descriptors most affected by spacers A and B are clearly evident in the analogs shown in Table 4. The effect of varying the lengths of spacers A and B on the conformational flexibility of the resulting peptide is shown in Figure 7. The calculated "bioactive" conformers of these analogs are a loose α-helical or β-turn containing conformer (refer to Figures 6 and 7). Preliminary CD studies (data not shown) indicate that in aqueous buffer these analogs exhibit very strong characteristics of both β-turn and α-helical components.

It is of interest to point out that the positive charge at both the C- and N-terminus plays an effect on organism selectivity. Analysis of the data indicates that compound **2** is significantly more active against SA than compound **3**, while the activity of compounds **2** and **3** are identical against MR. Compound **3** has a free amine and, thus, a positive charge at the N-terminus, while in compound **2** the amine is acetylated. The presence of a positive charge at the N-terminus reduces the activity from 3 μM (compound **2**) to 10 μM (compound **3**). Extending this logic to include compound **4**, which differs from compound **2** by a having the free amine and a K residue (which introduces two positive charges at the N-terminus), reduces the activity even

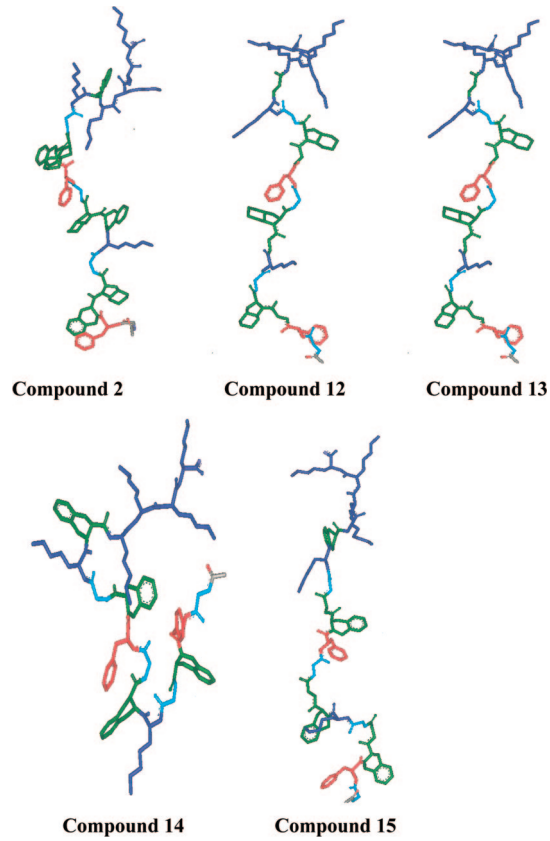

Figure 6. Calculated "bioactive conformers" for the analogs with the deletion of either the Tic or Oic residue indicate that these analogs are extended and do not include a helical or β-turn structure. The Tic−Oic dipeptide turn inducing unit is shown in green. The cationic residues are shown in dark blue. Hydrophobic residues are shown in red. Spacers A and B are shown in light blue.

Table 4. Descriptors most Affected by Spacers A and B

	cmpd **2**		cmpd **7**		cmpd **8**		cmpd **9**		cmpd **11**		
cmpd	value	Δ%	value	Δ%	value	Δ%	value	Δ%	value	Δ%	Δ%
					Electrostatic Potential						
dipole-magnitude	269.596	0	222.841	−17.35	256.579	−4.82	220.357	−18.25	145.619	−45.99	45.99
F-charge	6.000	0	6.000	0	6.000	0	6.000	0	6.000	0	0
Jurs-FNSA-3	−0.051	0	−0.050	+1.96	−0.056	−9.8	−0.045	+11.76	−0.026	+9.0	+21.56
Jurs-RPSA	0.274	0	0.239	−12.77	0.268	−2.19	0.228	−16.79	0.210	−23.36	23.36
Jurs-FPSA-1	0.823	0	0.827	+0.49	0.805	−2.2	0.829	+0.73	0.834	+1.33	3.53
Jurs-PNSA-1	576.297	0	608.270	+5.55	704.141	+22.18	634.863	+10.16	528.652	−8.27	30.45
Jurs-PNSA-2	−15950.000	0	−17351.269	−8.78	−19787.484	−24.055	−18648.209	−16.91	−6814.498	−57.27	+51.27
Jurs-PPSA-1	2672.174	0	2911.683	+8.94	2899.114	+8.5	3086.010	+15.5	2661.015	−0.415	+15.92
Jurs-RPCG	0.013	0	0.013	0	0.013	0	0.012	0	0.013	0	0
					Molecular Shape						
density	1.054	0	1.043	−1.0	1.047	−0.66	1.031	−2.18	1.042	−1.13	2.18
H-bond acceptor	20.000	0	20.000	0	20.000	0	20.000	0	16.000	−20	20
Jurs-RASA	0.726	0	0.761	+4.8	0.732	+0.83	0.772	+6.33	0.790	+8.8	8.80
H-bond donor	32.000	0	32.000	0	32.000	0	32.000	0	28.000	−12.5	12.50
Rad-of-gyration	14.550	0	13.153	−9.6	14.228	−2.2	14.161	−2.67	11.799	−18.9	18.90
Rotl-bonds	78.000	0	86.000	+10.25	82.000	+5.13	94.000	+20.52	66.000	−15.38	35.90
					Amphipathicity						
Jurs-RASA	0.726	0	0.761	+4.8	0.732	+0.83	0.772	+6.33	0.790	+8.8	8.80
Jurs-RPSA	0.274	0	0.239	−12.77	0.268	−2.12	0.228	−16.79	0.210	−23.36	23.36
AlogP	−3.252	0	−1.520	53.26	−2.527	22.3	1.650	49.3	1.054	67.56	67.56

more to 30 μM. The effect of positive charge on bioactivity of SA QSAR model is about 34% [predominately from Jurs-FPSA-1 (29%), Jurs-DPSA-2 (3%) and Jurs-FPSA-3 (2%)], whereas the effect of positive charge on the bioactivity of the MR QSAR model is only about 19% [predominately from Jurs-PPSA-1 (15%), Jurs-FPSA-1 (3%), and Jurs-PPSA-1 (1%)]. Thus, the positive charge affects the SA bioactivity twice as much as it affects the MR bioactivity. This data and results explain the difference in activity between compound **2** and compound **3** with respect to SA and the identical activity of the same compounds with respect to MR.

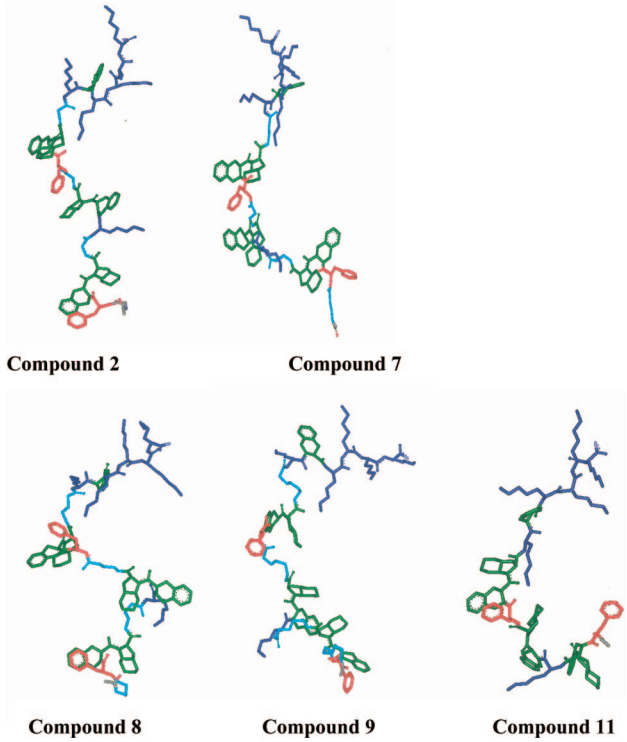

Figure 7. The calculated "bioactive" conformers of the analogs containing various length amino acid spacers in positions A and B indicate that these compounds adopt a helical or β-turn conformation. The Tic−Oic dipeptide turn inducing unit is shown in green. The cationic residues are shown in dark blue. Hydrophobic residues are shown in red. Spacers A and B are shown in light blue.

Table 5. Descriptors Relating Charge Density with SA Activity

percent contribution		+29%	−16%	−15%	+11%
cmpd	SA activity	Jurs-FPSA-1	density	Jurs-TASA	Jurs-PNSA-1
5	3	0.834	1.042	2520	528
6	3	0.837	1.037	2761	564
effect on bioactivity		increase BA	increase BA	decrease BA	decrease BA

Table 6. Descriptors Relating Charge Density with MR Activity

percent contribution		−30%	+16%	−15%	+10%
cmpd	MR activity	density	Jurs-RASA	Jurs-PPSA-1	Jurs-TPSA-1
5	30	1.043	0.791	2668.13	670.01
6	3	1.037	0.794	2919.12	717.85
effect on bioactivity		increase BA	increase BA	decrease BA	increase BA

Increasing the number of Lys residues at the C-terminus also plays a role in organism selectivity. Compound **5** has four K residues at the C-terminus, with a MR activity of 30 μM and compound **6** has six K residues at the C-terminus, with a MR activity of 3 μM. The same trend holds true for compounds **7** and **10**. Compound **7** has four K residues at the C-terminus, with a MR activity of 10 μM and compound **10** has five K residues at the C-terminus with a MR activity of 3 μM. As can be seen from Table 5, the physicochemical properties Jurs-FPSA-1 and density cause an increase in the SA bioactivity from compound **5** to compound **6**, but physicochemical properties Jurs-TASA and Jurs-PNSA-1 cause a decrease in the SA bioactivity from compound **5** to compound **6**. Thus, this cancellation effect is manifested in the equal activity of compound **5** and compound **6** against SA. As can be seen from Table 6, the physicochemical properties density, Jurs-RASA, and Jurs-TPSA-1 cause an increase in the MR bioactivity from compound **5** to compound **6**, but physicochemical property Jurs-PPSA-1 causes only a marginal decrease in the MR bioactivity from compound **5** to compound **6**. Thus, the net effect is manifested in the increased bioactivity of compound **6** as compared to that of

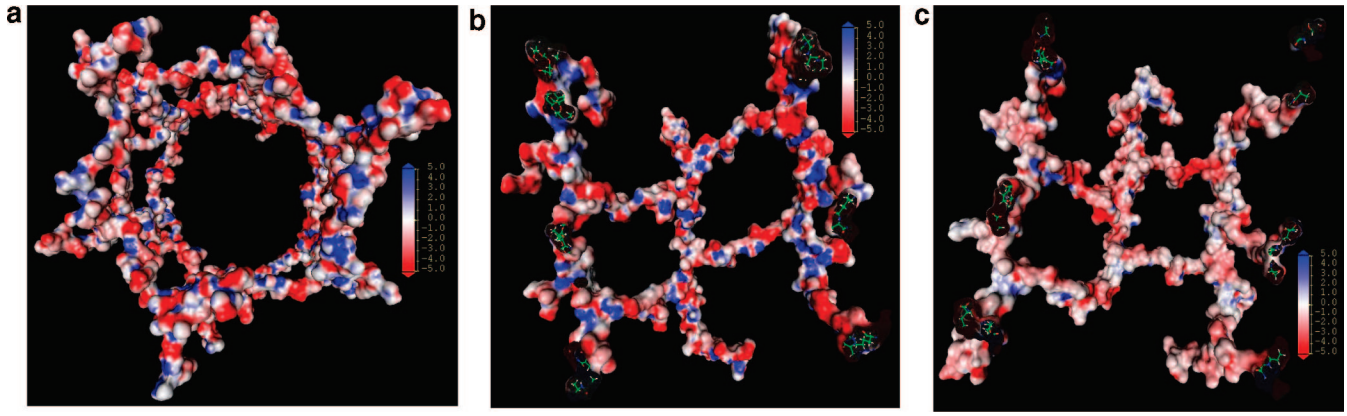

Figure 8. (a) Top down view into the hexagonal pore form of SA peptidoglycan outer layer showing a highly-charged polar surface. (b, c) Views from inside of the pore looking at two internal faces of the pore: (b) looking toward the highly-charged polar face and (c) looking at the relatively nonpolar opposite face. Color coding: blue indicates positive potential, red indicates negative potential, and white indicates neutral potential.

compound **5** against SA. In summary, even a small change, such as addition of a single Lys, has an effect on all the physicochemical properties of the peptide. The cumulative effect of this difference in physicochemical properties results in the large differences in observed bioactivity, as shown by the example of compounds **5** and **6**.

Recently, Meroueh et al.[32] reported the three-dimensional structure of bacterial cell wall peptidoglycan of SA, which concurs with the previously reported observations that the SA peptidoglycan outer layer is distinctly anionic.[33] Thus, for the electrostatic interactions occurring between the target (SA) cell's membrane and the peptide, the organism potency is determined, and it is a necessary condition for any active AMP to provide a complimentary polar face for the initial electrostatic attraction. The ESP maps of the inner faces of the hexagonal units of SA cell membrane (Figure 8a−c) show that about half of the inner surface is distinctly polar, while the opposite half is distinctly nonpolar. This figure illustrates two major points: (1) the peptidoglycan presents a highly charged polar face to the approaching AMP and (2) once bound to the surface of the peptidoglycan presents an amphipathic pore to the AMP, which is very complimentary to its own amphipathic character. Also, it is known that the SA outer cell membrane pore size measures ∼70–100 Å,[32] and we have found that the largest dimension of these bioactive AMPs is about 30–40 Å. Thus, one can rationally speculate that this amphipathic pore may play a role in transporting AMPs through the peptidoglycan layer to the lipid bilayer of the membrane propelled by the complementarity of electrostatics between AMPs and the SA peptidoglycan layer.

The molecular modeling results presented herein unequivocally demonstrate that different physicochemical descriptors for the same antimicrobial peptide define different antibacterial activity against these two different bacterial strains. Further more, these results coupled with the calculated electrostatic surface potential maps for the peptidoglycan clearly indicate that the physicochemical interactions that occur between AMP membrane-disruptors and their target cells control organism selectivity and potency. It is therefore critical, for future development and understanding of AMPs, to include the effects of these 3D physicochemical properties in any investigation of AMP membrane/cell interactions.

Equations

SA QSAR Model is Described by the Following Equation: 1. SA predicted activity = [(−1.49592 × "Fcharge") + (0.0098147 × "dipole-mag") + (0.013993 × "Jurs-SASA") + (0.00233 × "Jurs-PPSA-1") + (0.187647 × "Jurs-PNSA-1") + (0.0021686 × "Jurs-PNSA-2") + (0.00036919 × "Jurs-DPSA-2") + (0.0015025 × "Jurs-DPSA-3") + (438.251 × "Jurs-FPSA-1") + (267.258 × "Jurs-FPSA-3") + (120.432 × "Jurs-FNSA-3") − (715.316 × "Jurs-RPCG") − (12.8649 × "Jurs-RPCS") − (0.065752 × "Jurs-TASA") − (125.513 × "Jurs-RPSA") + (125.513 × "Jurs-RASA") − (183.99 × "density") + (1.03397 × "Hbond acceptor") + (0.039473 × "Hbond donor") − (0.306856 × "Rotlbonds") + (0.114808 × "AlogP") − (0.10004 × "RadOfGyration") − 225.589].

MR QSAR Model is Described by the Following Equation: 2. MR predicted activity = [(−0.0083585 × "conformer energy") + (2.05758 × "Fcharge") + ($5.3259e^{-05}$ × "Apol") + (0.0061422 × "dipole-mag") − (0.023941 × "Jurs-PPSA-1") − (0.008252 × "Jurs-PNSA-1") + ($5.5381e^{-05}$ × "Jurs-PPSA-2") + (0.00018566 × "Jurs-PNSA-2") − (18.282 × "Jurs-FPSA-1") + (13.321 * "Jurs-FNSA-3") − (8.46841 × "Jurs-RPCG") + (66.6262 × "Jurs-RNCG") + (0.052889 × "Jurs-TPSA") − (96.9761 × "Jurs-RPSA") + (96.9761 × "Jurs-RASA") − (127.577 × "density") + (0.768698 × "Hbond acceptor") − (0.498282 × "Hbond donor") − (0.060764 × "Rotlbonds") − (0.075759 × "AlogP") + (0.337835 × "RadOfGyration") + 110.841].

Acknowledgment. The authors would like to acknowledge funding from the Bacterial Therapeutics Program 2.1 of the Defense Threat Reduction Agency. This research was performed while one of the authors (J.B.B.) held a National Research Council Research Associateship Award at Walter Reed Army Institute of Research. The authors are grateful to Prof. Shahriar Mobashery from the Department of Chemistry and Biochemistry at the University of Notre Dame, IN, for providing the *Staphylococcus aureus* peptidoglycan cell wall coordinates. Material has been reviewed by the Walter Reed Army Institute of Research. There is no objection to its presentation or publications. The opinions or assertions contained herein are the private views of the authors and are not to be construed as official or as reflecting true views of the Department of the Army

or the Department of Defense. Material in this document is covered by U.S. Provisional Patent Application number 60/876,377, assigned to the United States Army.

Supporting Information Available: Additional data tables. This material is available free of charge via the Internet at http://pubs.acs.org.

References

(1) Dennison, S. R.; Wallace, J.; Harris, F.; Phoenix, D. A. Amphiphilic α-helical antimicrobial peptides and their structure/function relationships. *Protein Pept. Lett.* **2005**, *12*, 31–39.

(2) Yeaman, M. R.; Yount, N. Y. Mechanisms of antimicrobial peptide action and resistance. *Pharmacol. Rev.* **2003**, *55* (1), 27–55.

(3) Hancock, R. E. W. The therapeutic potential of cationic peptides. *Exp. Opin. Invest. Drugs* **1998**, *7*, 167–174.

(4) Toke, O. Antimicrobial peptides; new candidates in the fight against bacterial infections. *Biopolymers* **2005**, *80*, 717–735.

(5) Zasloff, M. Antimicrobial peptides of multicellular organisms. *Nature* **2002**, *415*, 389–395.

(6) Powers, J.-P. S.; Hancock, R. E. W. The relationship between peptide structure and antibacterial activity. *Peptides* **2003**, *24*, 1681–1691.

(7) Brogden, K. A. Antimicrobial peptides: Pore formers or metabolic inhibitors in bacteria. *Nat. Rev. Microbiol.* **2005**, *3*, 238–250.

(8) Blondelle, S. E.; Lohner, K.; Aguilar, M.-I. Lipid-induced conformation and lipid-binding properties of cytolytic and antimicrobial peptide: Determination and biological specificity. *Biochim. Biophys. Acta* **1999**, *1462*, 89–108.

(9) Hicks, R. P.; Mones, E.; Kim, H.; Koser, B. W.; Nichols, D. A.; Bhattacharjee, A. K. Comparison of the conformation and electrostatic surface properties of magainin peptidesbound to SDS and DPC micelles: Insight into possible modes on antimicrobial activity. *Biopolymers* **2003**, *68*, 459–470.

(10) Papo, N.; Shai, Y. Can we predict biological activity of antimicrobial peptides from their interaction with model phospholipid membranes. *Peptides* **2003**, *24*, 1693–1703.

(11) Papo, N.; Shai, Y. New lytic peptides based on the D,L amphipathic helix motif preferentially kill tumor cells compared to normal cells. *Biochemistry* **2003**, *42*, 9346–9354.

(12) Giangaspero, A.; Sandri, L.; Tossi, A. Amphipathic α-helical antimicrobial peptides. *Eur. J. Biochem.* **2001**, *268*, 5589–5600.

(13) Azuma, I.; Yamamura, Y.; Tanaka, Y.; Kohsaka, K.; Mori, T.; Itoh, T. Cell wall of *Mycobacterium lepraemurium* strain HI. *J. Bacteriol.* **1973**, *113* (1), 515–518.

(14) *Cerius2, Version 4.10L, QSAR Manual*; Accelrys Software Inc.: San Diego, CA, 2005; p 19.

(15) Marsili, M.; Gasteiger, J. Fast calculation of atomic charges from molecular topology and orbital electronegativies. *Stud. Phys. Theor. Chem.* **1981**, *16*, 56–67.

(16) Mayo, S. L.; Olafson, B. D.; Goddard, W. A. I. DREIDING: A generic force field. *J. Phys. Chem.* **1990**, *94*, 8897–8909.

(17) Hicks, R. P.; Bhonsle, J. B.; Venugopal, D.; Koser, B. W.; Magill, A. J. De novo design of selective antibiotic peptides by incorporation of un-natural amino acids. *J. Med. Chem.* **2007**, *50* (13), 3026–3036.

(18) Levitt, M.; Lifson, S. Refinement of protein conformations using a macromolecular energy minimization procedure. *J. Mol. Biol.* **1969**, *46* (2), 269–279.

(19) Chang, G.; Guida, W. C.; Still, W. C. An internal-coordinate Monte Carlo method for searching conformational space. *J. Am. Chem. Soc.* **1989**, *111*, 4379–4386.

(20) Performing a conformational analysis. *Cerius2, Version 4.10L, Conformational Search and Analysis Manual*; Accelrys Software Inc.: San Diego, CA, 2005; p 49.

(21) Bhonsle, J. B.; Wang, Z. W.; Tamamura, H.; Fujii, N.; Peiper, S. C.; Trent, J. O. A simple, automated quasi-4D-QSAR, quasi-multiway PLS approach to develop highly predictive QSAR models for highly flexible CXCR4 inhibitor cyclic pentapeptide ligands using scripted common molecular modeling tools. *QSAR Comb. Sci.* **2005**, *24* (5), 620–630.

(22) Bhonsle, J. B. *Cerius2, conformation search and analysis*, 2005; unpublished.

(23) Wold, H., *Partial Least Squares*; Wiley: New York, 1985; Vol. 6, pp 581–591.

(24) Bro, R. Multiway calibration. Multilinear PLS. *J. Chemom.* **1996**, *10*, 47–61.

(25) Hasegawa, K.; Arakawa, M.; Funatsu, K. 3D-QSAR study of insecticidal neonicotinoid compounds based on 3-way partial least squares model. *Chemom. Intell. Lab. Syst.* **1999**, *47*, 33–40.

(26) Bhonsle, J. B., unpublished results.

(27) L'Heureux, P. J.; Carreau, J.; Bengio, Y.; Delalleau, O.; Yue, S. Y. Locally linear embedding for dimensionality reduction in QSAR. *J. Comput.-Aided Mol. Des.* **2004**, *18*, 475–482.

(28) Olah, M.; Bologa, C.; Oprea, T. L. An automated PLS search for biologically relevant QSAR descriptors. *J. Comput.-Aided Mol. Des.* **2004**, *18*, 437–449.

(29) Yao, S. W.; Lopes, V. H. C.; Fernandez, F.; Garcia-Mera, X.; Morales, M.; Rodriquez-Borges, J. E.; Corderio, M. N. D. S. Synthesis and QSAR study of the anticancer activity of some novel indane carbocyclic nucleosides. *Bioorg. Med. Chem.* **2003**, *11* (23), 4999–5006.

(30) Bhonsle, J. B.; Bhattacharjee, A. K.; Gupta, R. Novel semi-automated methodology for developing highly predictive QSAR models: application for development of QSAR models for insect repellent amides. *J. Mol. Model.* **2007**, *13* (1), 179–208.

(31) Topliss, J. G.; Edwards, R. P., Chance effects in QSAR studies. In *Computer-Aided Drug Design*; Olsen, E. C., Christofferson, R. E., Eds.; ACS Symposium Series, American Chemical Society: Washington, DC, 1979; Vol. 112, p 131.

(32) Meroueh, S. O.; Bencze, K. Z.; Hesek, D.; Lee, M.; Fisher, J. F.; Stemmler, T. L.; Mobashery, S. Three-dimensional structures of bacterial cell wall peptidoglycan. *Proc. Natl. Acad. Sci.* **2006**, *103* (12), 4404–4409.

(33) Hancock, R. E. Cationic antimicrobial peptides: Toward clinical applications. *Expert Opin. Investig. Drugs* **2000**, *8*, 1723–1729.

(34) White, S. H.; Wimley, W. C. Hydrophobic interactions of peptides with membrane interfaces. *Biochim. Biophys. Acta* **1998**, *1376* (3), 339–352.

JM070884Y